Supplemental Material:

Floquet engineering of black phosphorus upon below-gap pumping

Shaohua Zhou,[1,*] Changhua Bao,[1,*] Benshu Fan,[1,*] Fei Wang,[1] Haoyuan Zhong,[1]
Hongyun Zhang,[1] Peizhe Tang,[3,4,†] Wenhui Duan,[1,2,5] and Shuyun Zhou[1,2,‡]

[1]*State Key Laboratory of Low-Dimensional Quantum Physics and Department of Physics, Tsinghua University, Beijing 100084, China*

[2]*Frontier Science Center for Quantum Information, Beijing 100084, China*

[3]*School of Materials Science and Engineering, Beihang University, Beijing 100191, China*

[4]*Max Planck Institute for the Structure and Dynamics of Matter, Center for Free Electron Laser Science, 22761 Hamburg, Germany*

[5]*Institute for Advanced Study, Tsinghua University, Beijing 100084, China*

CONTENTS

In our time- and angle-resolved photoemission spectroscopy (TrARPES) measurements (see Appendix A), we have observed evidence for the Floquet transient electronic renormalization near the edge of the valence band in black phosphorus upon below-gap pumping, which shows strong pump polarization dependence (see Appendix B). We exclude the contribution of electron-hole pairs in the band renormalization (see Appendix C). We construct a light-induced Floquet effective $\mathbf{k}\cdot\mathbf{p}$ Hamiltonian $\hat{H}_{\Gamma}^{F-AC}(\mathbf{k}_{\parallel})$ around the Γ point in black phosphorus based on the Floquet theory (see Appendix D and E) and give some qualitative explanations of the momentum-dependent renormalization (see Appendix F). When the pumping energy is around 160 meV, the energy shift ΔE is proportional to the below-gap pump fluence (see Appendix G). We apply the Löwdin Partitioning approach to perform a perturbative analysis for the evolution of ΔE with the change of pumping photon energies in the non-resonant conditions (see Appendix H). Moreover, the origin of the unresolved calculated anti-crossing gap is discussed in Appendix I.

Appendix A: Methods

Single crystal growth

High quality black phosphorus single crystals were synthesized by the tin-iodine-assisted chemical vapor transport reaction. The red phosphorus lump (Alfa Aesar, 99.999%), tin grains (Aladdin, 99.99%), and iodine crystals (Alfa Aesar, 99.99%) were mixed in a vacuum-sealed silica ampoule. The ampoule was heated to 400℃ within 4 hours, then slowly heated to 600℃ within 10 hours and maintained at 600℃ for 1 day. After the reaction, the ampoule was slowly cooled to 350℃ from 600℃ at a cooling rate of 10℃/hour. Finally, black phosphorus single crystals were obtained after cooling to room temperature.

TrARPES measurements

The TrARPES measurements are performed using a home-bulit TrARPES systems based on a Ti:sapphire laser amplifier with center wavelength of 800 nm, pulse energy of 1.4 mJ, pulse duration of 35 fs and repetition rate of 10 kHz. The laser is split into two beams to generate the pump and probe pulses respectively. The MIR pump pulses are generated using the cascade optical parametric amplifier (OPA) and non-collinear differential frequency generation (NDFG). The probe pulses with photon energy of 6.2 eV are generated by the fourth harmonics generation process using three BBO crystals. The samples were cleaved in ultrahigh vacuum chamber with base pressure better than 5 $\times 10^{-11}$ Torr and measured at a temperature of 80 K. The TrARPES spectra were mainly measured along AC direction with pump laser polarized also along AC direction except data shown in Fig. 3, which were measured along the direction at 30° from the AC direction with *p-pol.* pump for observing stronger sidebands and tracing the light field in time domain.

First-principles Calculation

In this study, we utilized the Vienna *Ab initio* Simulation Package (VASP) [1] to perform density functional theory (DFT) calculations in order to simulate the electronic structure of black phosphorus in the absence of laser pumping. To achieve this, we employed the projector-augmented wave (PAW) pseudopotential [2] and the Perdew-Burke-Ernzerhof (PBE) type exchange-correlation functional [3], using a plane-wave basis set with an energy cutoff of 400 eV. Sampling of the Γ-centered k-point meshes was performed as $12 \times 12 \times 12$ in the Brillouin zone (BZ) of the primitive cell. We relaxed the atomic positions using a force criterion of 0.01 eV/Å and applied a convergence condition of 10^{-6} eV for the elec-

tronic self-consistent loop. The van der Waals (vdW) corrections [4, 5] were incorporated during both lattice relaxation and self-consistent electronic calculations. To calculate the direct band gap at the Z point, we employed the Heyd-Scuseria-Ernzerhof (HSE) hybrid functional [6], which gave a value of 0.33 eV consistent with our TrARPES experimental observations. We also constructed the tight-binding Hamiltonian $\hat{H}^{TB}(\mathbf{k})$ from the *ab initio* calculations using the Wannier90 code [7–9].

Floquet Hamiltonian

In our TrARPES experiments, we employed a linear polarized probe pulse with a duration of ~ 100 fs, approximately equivalent to four optical cycles of the pump pulse [10] at photon energy of 160 meV. During our simulations, we presumed that a non-equilibrium Floquet band could be established within a few optical cycles, which has been previously supported by calculations reliant on the time-dependent DFT [11, 12]. As a consequence, the conditions for the application of the Floquet theory to evaluate the band structures of black phosphorus under such laser pumping were deemed satisfactory.

In this work, we derived a time-dependent tight-binding Hamiltonian utilizing the Peierls substitution $\hat{H}^{TB}(\mathbf{k}) \rightarrow \hat{H}^{TB}(\mathbf{k} + \frac{e}{\hbar}\mathbf{A}(t))$, which employed the vector potential $\mathbf{A}(t) = (A_0 \sin\omega t, 0, 0)$ or $(0, A_0 \sin\omega t, 0)$ of the pumping laser with the frequency $\omega = 2\pi/T$. The electric field strength are adjusted appropriately to make the calculated results comparable with the experimental data whose values are 7.1×10^7 V/m in Fig. 2, 4 and 3.4×10^7 V/m in Fig. 3.

By applying the Floquet theory, the time-dependent Schrödinger equation $\hat{H}^{TB}(\mathbf{k}, t)\Psi^F_\gamma(t) = i\frac{\partial}{\partial t}\Psi^F_\gamma(t)$ with a time-periodic Hamiltonian $\hat{H}^{TB}(\mathbf{k}, t) = \hat{H}^{TB}(\mathbf{k}, t + T)$ has the following form of the wavefunction

$$\Psi^F_\gamma(t) = e^{-i\epsilon_\gamma t}\Phi_\gamma(t) \tag{1}$$

where ϵ_γ is known as Floquet quasienergy and $\Phi_\gamma(t) = \Phi_\gamma(t + T)$ is the time-periodic function. We then expanded $\Phi_\gamma(t)$ in Eq.(1) with respect to a complete set $\{u^m_\gamma\}$ as

$$\Phi_\gamma(t) = \sum_{m=-\infty}^{\infty} e^{-im\omega t}u^m_\gamma \tag{2}$$

then inserted Eq.(1) and Eq.(2) into the original Schrödinger equation, integrated against $e^{in\Omega t}$ on both sides of the equation and obtained the eigenvalue equation

$$\sum_m \hat{H}^{FTB}_{n,m}(\mathbf{k})u^m_\gamma = \epsilon_\gamma u^n_\gamma \tag{3}$$

where $\hat{H}^{FTB}_{n,m}(\mathbf{k}) = \frac{1}{T}\int_0^T dt \hat{H}^{TB}(\mathbf{k},t)e^{i(n-m)\omega t} - m\omega\delta_{mn}$. The index γ labels eigenstates and m, n are the Fourier mode indices. Herein, the Floquet theory transforms the time-dependent Schrödinger equation into a static eigenvalue equation within an extended Hilbert space. We can diagonalize $\hat{H}^{FTB}(\mathbf{k})$ to obtain the Floquet band structure of the black phosphorus under the laser pumping, and finally the evolution of the wavefunction in the black phosphorus can be expanded by Floquet states as $\Psi(t) = \sum_\gamma C_\gamma \Psi^F_\gamma(t)$.

Appendix B: Pump polarization dependence of Floquet band renormalization

The impact of below-gap pumping on the Floquet band renormalization in black phosphorus is found to display a polarization dependence similar to that observed in near-resonance pumping. Specifically, the pump laser which is polarized along armchair (AC) direction can induce stronger renormalization. As shown in Fig. S1b,c, the below-gap pumping laser can induce a remarkable band renormalization at the valence band edge, which is also supported by the Floquet tight-binding simulations (Fig. S1d). However, as for the pumping laser with the polarization along the zigzag (ZZ) direction, the renormalization effect is strongly reduced (Fig. S1f-h). The observed pump polarization dependence for the band renormalization is linked to the pseudospin degree of freedom in black phosphorus [13] and summarized in Fig. S1i,j.

In the experiment, the pump polarization is changed while fixing the measurement direction along AC direction, as schematically illustrated in Fig. S1a,e. For these two cases, the transmitted electric field is calculated as follows. The refractive index n is evaluated to be 3.4 from the reflectance at the photon energy of 160 meV (30%) [14] for both polarizations along AC and ZZ directions. According to the Fresnel equation with the incident angle of 54°, the transmissivity of the electronic field for AC pump (s-pol.) and ZZ pump (p-pol.) are $t_s = 0.3$ and $t_p = 0.4$ respectively, so the transmitted electric field for ZZ pump is even larger than that of AC pump. Therefore, the observed stronger renormalization for AC pump is not caused by the transmitted electric field, but rather it is intrinsically linked to the selection rule instead of the change of reflection. Moreover, owing to the out-of-plane electric field component for $p-pol.$ pump polarization, the dressed electronic states also have contributions from the Volkov states which are light-dressed photoemission final states, and stronger sidebands are observed due to the interference between Floquet and Volkov

states [15]. Nevertheless, this does not change the conclusion that the light-induced change in the electronic structure is caused by Floquet band engineering, because Volkov states do not lead to band renormalization.

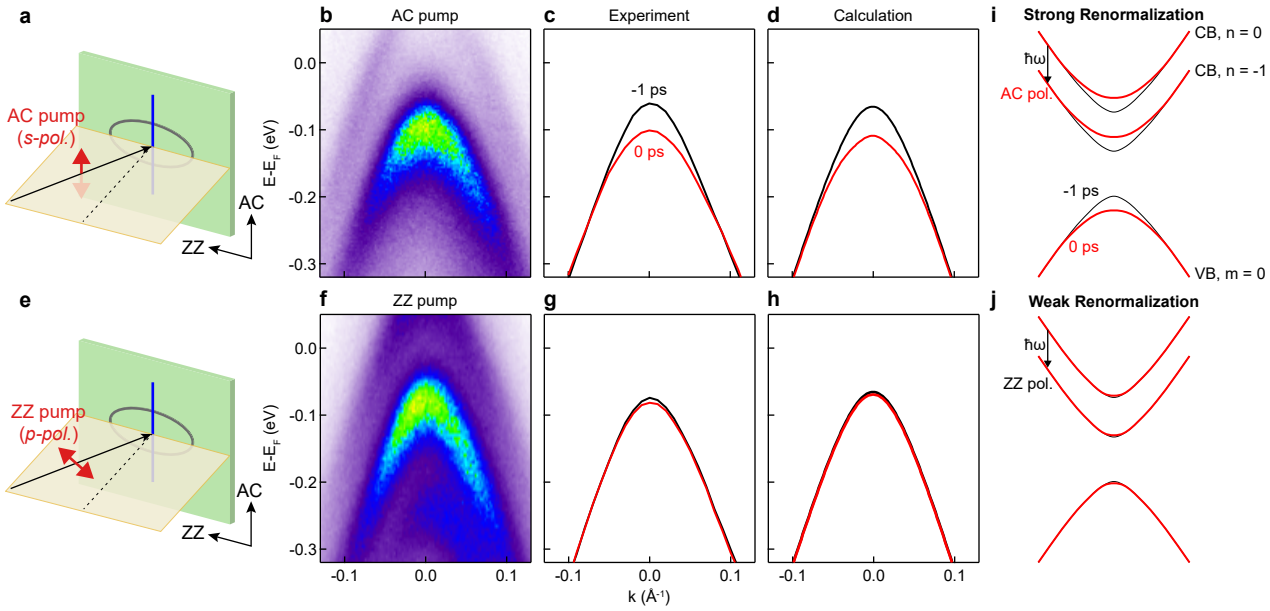

FIG. S1. **Pump polarization dependence of Floquet band renormalization a**, Schematics for experimental geometry of AC pump. **b**, TrARPES dispersion of black phosphorus along AC direction with the polarization along the AC direction at the delay time of $\Delta t = 0$. The pump photon energy is 160 meV and the pump fluence is 500 μJ/cm^2. **c**, The extracted dispersions at $\Delta t = 0$ ps (red line) and corresponding data at $\Delta t =$ -1 ps (black line). **d**, Calculated dispersions based on Floquet tight-binding simulations at $\Delta t = 0$ ps (red line) and $\Delta t =$ -1 ps (black line). **e-h**, Similar results as **a-c** but with the polarization of pumping laser along the ZZ direction. **i,j**, Schematic summary of the polarization dependence of Floquet band engineering on below-gap pumping.

Appendix C: Suppressed optical absorption by below-gap pumping

First, from the optical absorption spectra, the optical absorption of black phosphorus is largely suppressed for below-gap photoexcitation, especially at 160 meV [16]. Secondly, analysis of the TrARPES shows that population of the CB is negligible upon below-gap

pumping. For above-gap pumping with $\hbar\omega$=370 meV, CB is clearly observed (pointed by the red arrow in Fig. S2e), suggesting that CB is populated upon above-gap pumping as expected. When decreasing the pump photon energy to below-gap pumping region, the CB intensity is strongly reduced (Fig. S2b,c, see also EDC analysis in Fig. S2f). Both of these suggest that the light-induced change upon below-gap pumping is not caused by the electron-hole pair creation.

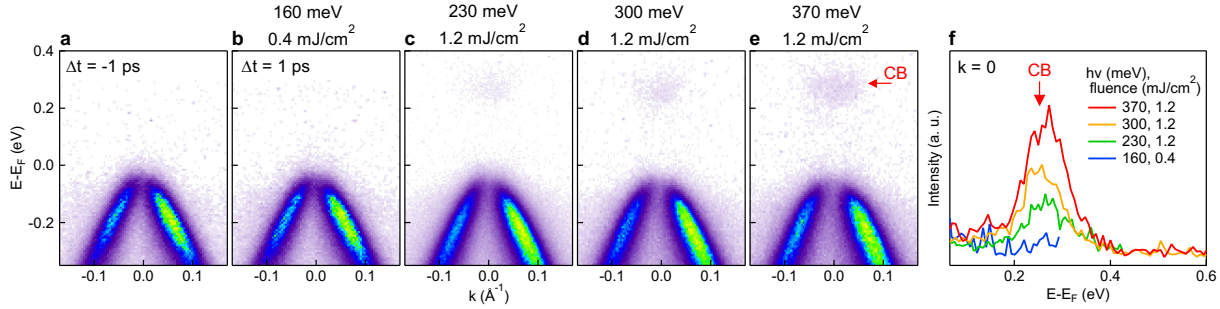

FIG. S2. **Population of CB for below-gap and above-gap pumping a** TrARPES spectra at the delay time of Δt = -1 ps. **b-e** TrARPES spectra with different pump photon energies at the delay time of Δt = 1 ps. **f** EDCs at the Γ point extracted from the data shown in b-e. The pump polarization is along the AC direction (s-pol.) and the probe polarization is along the ZZ direction.

Appendix D: Effective $\mathbf{k}\cdot\mathbf{p}$ Hamiltonian around the Γ point in equilibrium

In black phosphorus, the optical absorption between the valence band maximum (VBM) and conduction band minimum (CBM) only occurs for the pumping laser along the AC direction [13]. This leads to the dipole matrix elements γ_1 and γ_2 taking the form:

$$\begin{aligned}\gamma_1 &= \langle c|AC|v\rangle \neq 0\\ \gamma_2 &= \langle c|ZZ|v\rangle = 0\end{aligned} \tag{4}$$

where $|v\rangle$ and $|c\rangle$ represent the electronic states at VBM and CBM around the Γ point.

According to Refs. [17, 18], the effective $\mathbf{k}\cdot\mathbf{p}$ Hamiltonian around the Γ point in the cleaved plane of black phosphorus takes a form similar to that of monolayer black phospho-

rus:

$$\hat{H}_{\Gamma}(\mathbf{k}_{\parallel}) = \begin{pmatrix} E_c + \eta_c k_y^2 + \nu_c k_x^2 & \gamma_1 k_y \\ \gamma_1^* k_y & E_v + \eta_v k_y^2 + \nu_v k_x^2 \end{pmatrix} \tag{5}$$

Here, k_x and k_y are the momenta along the ZZ and AC directions, $E_c = 0.165$ eV and $E_v = -0.165$ eV are the energy levels for the CBM and VBM at the Γ point, and η_c, ν_c, η_v and ν_v are the band parameters with values of -2.519 eV·Å^2, 3.225 eV·Å^2, -1.512 eV·Å^2 and -2.982 eV·Å^2, respectively. The module value of the optical matrix element $\gamma_1 = \langle c|AC|v\rangle$ is 3.691 eV·Å and $\gamma_2 = \langle c|ZZ|v\rangle = 0$.

Appendix E: The linear polarized pumping laser with AC polarization

We consider a linearly polarized pumping laser with oscillation along the AC direction and apply the Peierls substitution, $k_y \rightarrow k_y + eA\cos\omega t/\hbar$, to obtain the time-dependent effective $\mathbf{k}\cdot\mathbf{p}$ Hamiltonian $\hat{H}_{\Gamma}(t, \mathbf{k}_{\parallel})$ as

$$\hat{H}_{\Gamma}(t, \mathbf{k}_{\parallel}) = \begin{pmatrix} E_c + \eta_c k_y^2 + \nu_c k_x^2 + 2e\eta_c k_y A\cos\omega t/\hbar & \gamma_1 k_y + e\gamma_1 A\cos\omega t/\hbar \\ \gamma_1^* k_y + e\gamma_1^* A\cos\omega t/\hbar & E_v + \eta_v k_y^2 + \nu_v k_x^2 + 2e\eta_v k_y A\cos\omega t/\hbar \end{pmatrix} \tag{6}$$

where e is the charge of electron, $\hbar$ is the reduced Planck constant and A denotes the vector potential of the pumping laser calculated via E_0/ω. We set the electric field E_0 to 7.1×10^7 V/m and the photon energy $\hbar\omega$ to 160 meV for the following calculations. Then the Floquet theory is employed to obtain the Floquet matrix elements $\left[\hat{H}_{\Gamma}^{F-AC}(\mathbf{k}_{\parallel})\right]_{nm}$ as

$$\begin{aligned} &\left[\hat{H}_{\Gamma}^{F-AC}(\mathbf{k}_{\parallel})\right]_{nm} \\ =&\frac{1}{T}\int_0^T dt \hat{H}_{\Gamma}(t, k_{\parallel}) e^{i(n-m)\omega t} - m\hbar\omega\delta_{mn} \\ =&\begin{pmatrix} (E_c+\eta_c k_y^2+\nu_c k_x^2 - m\hbar\omega)\delta_{mn} + \frac{e\eta_c k_y E_0}{\hbar\omega}(\delta_{m,n+1}+\delta_{m,n-1}) & \gamma_1 k_y \delta_{mn} + \frac{e\gamma_1 E_0}{2\hbar\omega}(\delta_{m,n+1}+\delta_{m,n-1}) \\ \gamma_1^* k_y \delta_{mn} + \frac{e\gamma_1^* E_0}{2\hbar\omega}(\delta_{m,n+1}+\delta_{m,n-1}) & (E_v+\eta_v k_y^2+\nu_v k_x^2 - m\hbar\omega)\delta_{mn} + \frac{e\eta_v k_y E_0}{\hbar\omega}(\delta_{m,n+1}+\delta_{m,n-1}) \end{pmatrix} \end{aligned} \tag{7}$$

where $T = 2\pi/\omega$ is an optical cycle of the pumping laser.

Herein, we just consider the lowest-order contributions of light-matter interaction within the framework of Floquet theory. By truncating the time-independent Floquet effective $\mathbf{k}\cdot\mathbf{p}$

Hamiltonian $\hat{H}_{\Gamma}^{F-AC}(\mathbf{k}_{\parallel})$ in Eq. 7 to $m, n = \{-1, 0, 1\}$, we obtain its form as

$$\hat{H}_{\Gamma}^{F-AC}(\mathbf{k}_{\parallel}) = \begin{pmatrix} E_c+\eta_c k_y^2+\nu_c k_x^2+\hbar\omega & \gamma_1 k_y & \frac{e\eta_c k_y E_0}{\hbar\omega} & \frac{e\gamma_1 E_0}{2\hbar\omega} & 0 & 0 \\ \gamma_1^* k_y & E_v+\eta_v k_y^2+\nu_v k_x^2+\hbar\omega & \frac{e\gamma_1^* E_0}{2\hbar\omega} & \frac{e\eta_v k_y E_0}{\hbar\omega} & 0 & 0 \\ \frac{e\eta_c k_y E_0}{\hbar\omega} & \frac{e\gamma_1 E_0}{2\hbar\omega} & E_c+\eta_c k_y^2+\nu_c k_x^2 & \gamma_1 k_y & \frac{e\eta_c k_y E_0}{\hbar\omega} & \frac{e\gamma_1 E_0}{2\hbar\omega} \\ \frac{e\gamma_1^* E_0}{2\hbar\omega} & \frac{e\eta_v k_y E_0}{\hbar\omega} & \gamma_1^* k_y & E_v+\eta_v k_y^2+\nu_v k_x^2 & \frac{e\gamma_1^* E_0}{2\hbar\omega} & \frac{e\eta_v k_y E_0}{\hbar\omega} \\ 0 & 0 & \frac{e\eta_c k_y E_0}{\hbar\omega} & \frac{e\gamma_1 E_0}{2\hbar\omega} & E_c+\eta_c k_y^2+\nu_c k_x^2-\hbar\omega & \gamma_1 k_y \\ 0 & 0 & \frac{e\gamma_1^* E_0}{2\hbar\omega} & \frac{e\eta_v k_y E_0}{\hbar\omega} & \gamma_1^* k_y & E_v+\eta_v k_y^2+\nu_v k_x^2-\hbar\omega \end{pmatrix} \tag{8}$$

Moreover, to obtain Floquet bands along the AC direction ($k_x = 0$) and ZZ direction ($k_y = 0$), we perform numerical simulations based on the Floquet effective $\mathbf{k} \cdot \mathbf{p}$ Hamiltonian $\hat{H}_{\Gamma}^{F-AC}(\mathbf{k}_{\parallel})$ in Eq. 8 and the light-induced Floquet transient renormalization is shown in Fig. S3. The calculated results are consistent with those obtained from the Floquet tight-binding model.

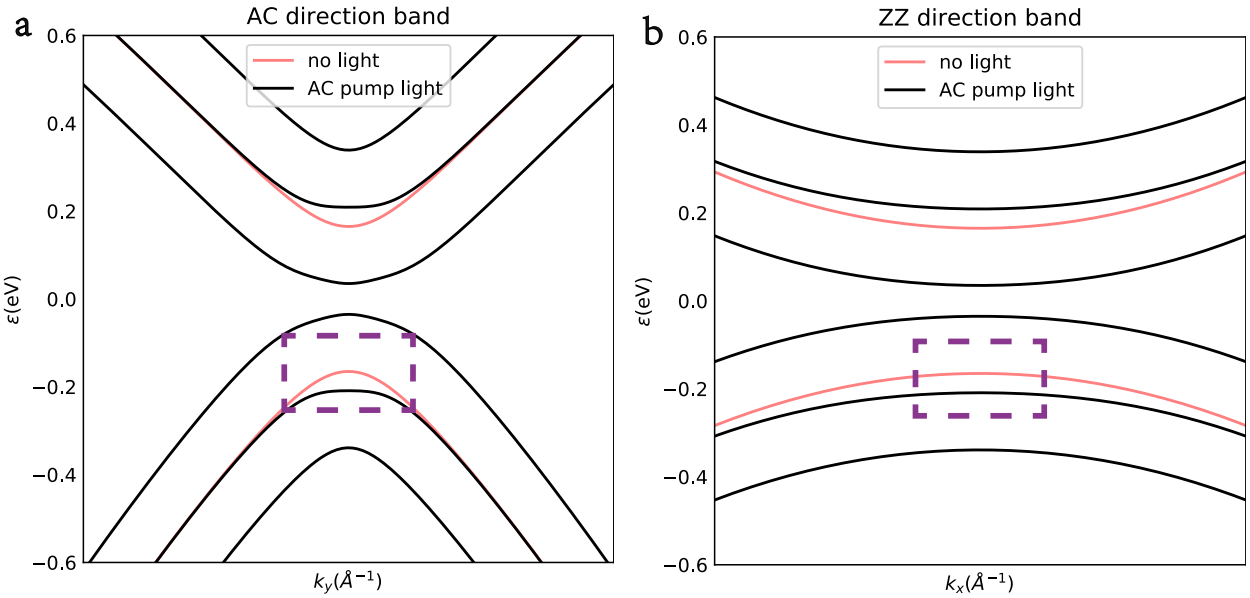

FIG. S3. **Theoretical calculation of Floquet band structure.** The Floquet band structures along (**a**) AC direction and (**b**) ZZ direction from the Floquet effective $\mathbf{k} \cdot \mathbf{p}$ Hamiltonian $\hat{H}_{\Gamma}^{F-AC}(\mathbf{k}_{\parallel})$ in Eq. 8 are shown in black lines. The pump polarization is along the AC direction and the Fermi level is set as zero.

Appendix F: Insight of the momentum-dependent renormalization

In order to give some qualitative explanations of the momentum-dependent renormalization upon below-gap pumping in our experiment, we first calculate the energy shift ΔE for the valence band edge around Γ point along the AC direction as shown in Fig. S4. We can clearly observe that ΔE strongly depends on the momentum. Generally speaking, this phenomenon could be roughly understood based on the perturbation theory. For semiconductors such as black phosphorous, the band dispersions are parabolic for the conduction band (CB) edge and valence band (VB) edge. Away from the band minimum of a direct-gap semiconductor (e.g., Γ point in black phosphorous), the energy difference between CB and VB, $E_g(k) = E_c(k) - E_v(k) = E_g + (m_c - m_v)k^2$ becomes larger, where E_g is the band gap at the Γ point, $m_{c(v)}$ is the effective mass for CB and VB edges, and k is the momentum. Based on the perturbation theory, the energy renormalization $\Delta E(k)$ should be inversely proportional to $E_g(k)$ approximately. Therefore, away from the Γ point, $E_g(k)$ becomes larger and $\Delta E(k)$ becomes smaller.

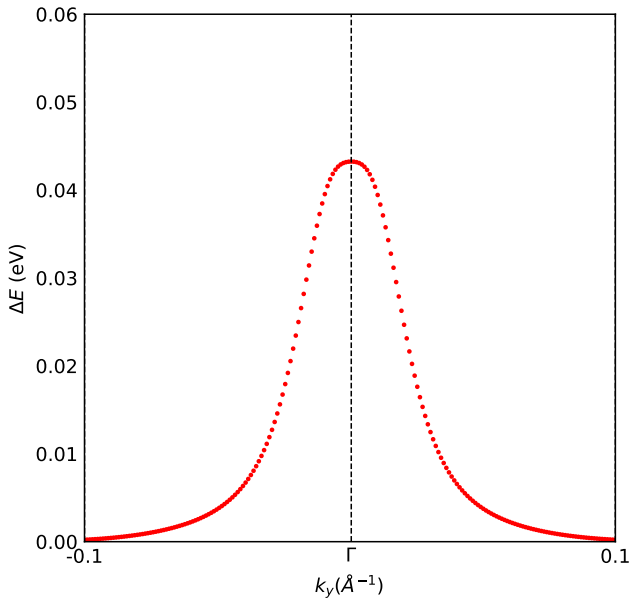

FIG. S4. **The energy shift ΔE for the valence band edge around Γ point.** Herein, we fix $E_0 = 7.1 \times 10^7$ V/m and $\hbar\omega = 0.16$ eV. The largest band shift can be observed at the Γ point.

Moreover, the off-diagonal block terms of the Floquet effective Hamiltonian in Eq. 8, which correspond to the light-matter interactions, are k_y-dependent and highly anisotropic

(see γ_1-dependent terms). Considering that the band shift ΔE results from these off-diagonal terms, we can conclude that the orbital characters of the valence and conduction bands together with the crystal symmetry in black phosphorous strongly affect the momentum-dependent band renormalization in black phosphorous.

Appendix G: Pump fluence dependence of Floquet band renormalization

The TrARPES spectra at $\Delta t = 0$ with different pump fluence are shown in Fig. S5a-h. Extracting the dispersions and energy distribution curves (EDCs) at the Γ point, we can observe that the band renormalization becomes larger with the higher pump fluence (Fig. S5i, j). Furthermore, the energy shift ΔE of Floquet band renormalization for valence band edge at the Γ point scales linearly with the pump fluence shows overall consistent with the linear dependence (the red dashed line in Fig. S5k) as predicated by the perturbative analysis for ΔE with low energy and small pump fluence in Appendix H.

Appendix H: Löwdin Partitioning for Floquet effective $\mathbf{k}\cdot\mathbf{p}$ Hamiltonian $\hat{H}_\Gamma^{F-AC}(\mathbf{k}_\parallel)$

In this part, we focus on the evolution of the energy shift ΔE at the Γ point with the change of photon energy $\hbar\omega$ upon below-gap pumping, where ΔE is defined as the difference between the VBM before and after laser pumping. The Floquet effective $\mathbf{k}\cdot\mathbf{p}$ Hamiltonian $\hat{H}_\Gamma^{F-AC}$ at the Γ point under a AC pumping has the form

$$\hat{H}_\Gamma^{F-AC} = \begin{pmatrix} E_v+\hbar\omega & \frac{e\gamma_1^* E_0}{2\hbar\omega} & 0 & 0 & 0 & 0 \\ \frac{e\gamma_1 E_0}{2\hbar\omega} & E_c & 0 & 0 & \frac{e\gamma_1 E_0}{2\hbar\omega} & 0 \\ 0 & 0 & E_v & \frac{e\gamma_1^* E_0}{2\hbar\omega} & 0 & \frac{e\gamma_1^* E_0}{2\hbar\omega} \\ 0 & 0 & \frac{e\gamma_1 E_0}{2\hbar\omega} & E_c-\hbar\omega & 0 & 0 \\ 0 & \frac{e\gamma_1^* E_0}{2\hbar\omega} & 0 & 0 & E_v-\hbar\omega & 0 \\ 0 & 0 & \frac{e\gamma_1 E_0}{2\hbar\omega} & 0 & 0 & E_c+\hbar\omega \end{pmatrix} = \begin{pmatrix} \hat{H}_\Gamma^{4\times4} & V \\ V^\dagger & \hat{H}^{2\times2} \end{pmatrix} \quad (9)$$

This Hamiltonian is derived by rearranging the order of matrix elements of $\hat{H}_\Gamma^{F-AC}$ in Eq. 8 with $k_x = k_y = 0$. Then we focus on the 4×4 Hamiltonian $\hat{H}_\Gamma^{4\times4}$ in the upper block of $\hat{H}_\Gamma^{F-AC}$ in Eq. 9. Using the Löwdin perturbation [19] up to the second-order correction, we

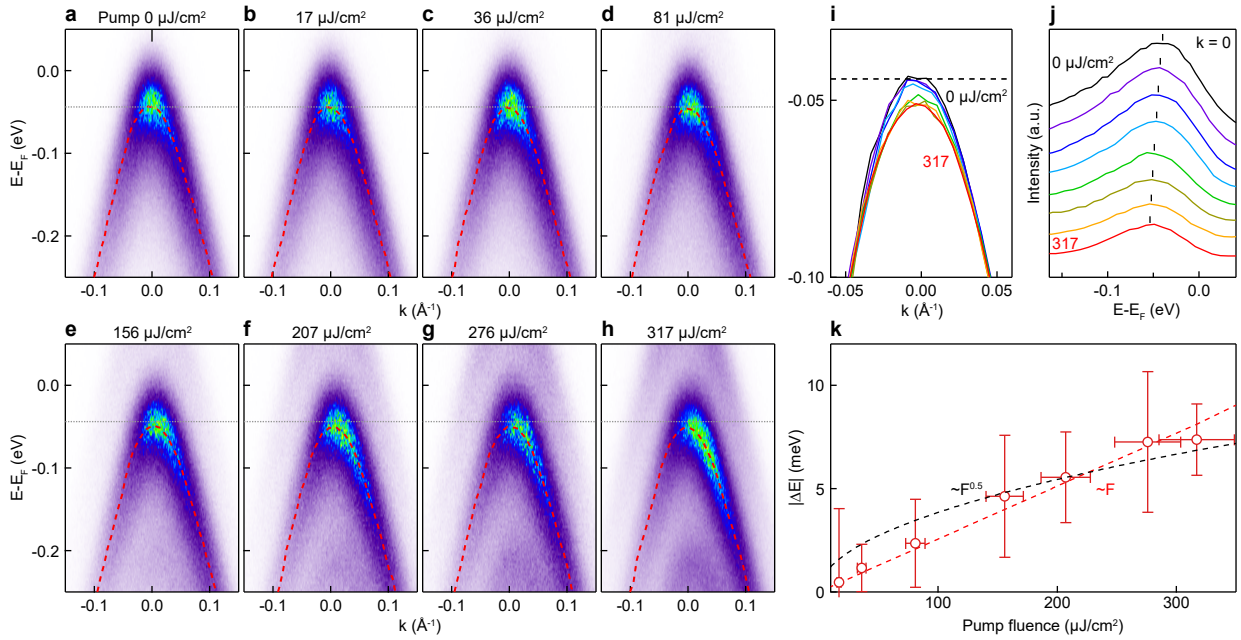

FIG. S5. **Pump fluence dependence of Floquet band renormalization a-h**, the TrARPES spectra with different pump fluence at the delay time of $\Delta t = 0$ with the pump photon energy of 160 meV. The red dashed lines and gray dotted lines indicate the extracted dispersions at $\Delta t = 0$ ps and the energy level of the Γ point at Δt = -1 ps. **i, j**, Extracted dispersions and EDCs at the Γ point using the data in **a-h**. **k**, Extracted the energy shift of band renormalization as a function of pump fluence. The error bars of the energy shift ΔE are extracted from the fitting results and the horizontal error bar of the pump fluence is defined by the actual fluctuation in the experiment with the ratio of 10%.

obtain the light-dressed effective Hamiltonian for $\hat{H}_{\Gamma}^{4\times4}$ as

$$\begin{pmatrix} E_v + \hbar\omega & \frac{e\gamma_1^* E_0}{2\hbar\omega} & 0 & 0 \\ \frac{e\gamma_1 E_0}{2\hbar\omega} & E_c + \frac{e^2|\gamma_1|^2 E_0^2}{4\hbar^2\omega^2(\hbar\omega+E_g)} & 0 & 0 \\ 0 & 0 & E_v - \frac{e^2|\gamma_1|^2 E_0^2}{4\hbar^2\omega^2(\hbar\omega+E_g)} & \frac{e\gamma_1^* E_0}{2\hbar\omega} \\ 0 & 0 & \frac{e\gamma_1 E_0}{2\hbar\omega} & E_c - \hbar\omega \end{pmatrix} \tag{10}$$

where $E_g = E_c - E_v = 0.33$ eV is the band gap of black phosphorus in equilibrium. Diagonalizing the Hamiltonian in Eq. 10, we obtain the energy shift ΔE as

$$\Delta E = \frac{\sqrt{\left(e^2|\gamma_1|^2E_0^2\right)^2 + \left(4\hbar^2\omega^2\left(E_g^2 - \hbar^2\omega^2\right)\right)^2 + 8e^2|\gamma_1|^2E_0^2\hbar^2\omega^2(E_g+\hbar\omega)(3E_g+\hbar\omega)}}{8\hbar^2\omega^2(E_g+\hbar\omega)} + \frac{e^2|\gamma_1|^2E_0^2 + 4\hbar^2\omega^2(\hbar^2\omega^2 - E_g^2)}{8\hbar^2\omega^2(E_g+\hbar\omega)} \tag{11}$$

Then we diagonalize the Hamiltonian $\hat{H}_\Gamma^{F-AC}$ (see Eq. 9) with different pumping photon energies and compare with ΔE obtained from Eq. 11. As shown in Fig. S6, these results are consistent, providing evidence for the validity of the Löwdin partitioning approach.

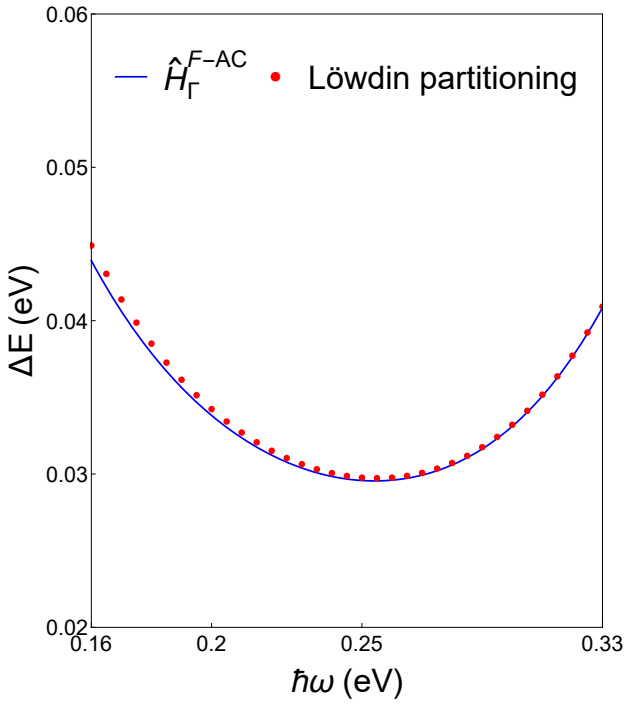

FIG. S6. **Comparison of the Löwdin partitioning approach for the energy shift.** Blue line for ΔE from the numerical diagonalization of the Hamiltonian $\hat{H}_\Gamma^{F-AC}$ and dotted red line for ΔE from the Löwdin partitioning approach.

To facilitate the subsequent perturbative analysis, we can make an order of magnitude estimation of terms shown in Eq. 11. In the setting of our experiments, $e^2|\gamma_1|^2E_0^2 \simeq 6.87 \times 10^{-4}$ $(eV)^4$ is estimated to be much small than $\sqrt{8e^2|\gamma_1|^2E_0^2\hbar^2\omega^2(E_g+\hbar\omega)(3E_g+\hbar\omega)}$ and $4\hbar^2\omega^2(E_g^2 - \hbar^2\omega^2)$ around 10^{-3} $(eV)^4$. So we can simplify ΔE in Eq. 11 by neglecting the

term $e^2|\gamma_1|^2E_0^2$ and obtain the energy shift ΔE as

$$\begin{aligned}\Delta E \simeq & \frac{\sqrt{\left(4\hbar^2\omega^2\left(E_g^2-\hbar^2\omega^2\right)\right)^2+8e^2|\gamma_1|^2E_0^2\hbar^2\omega^2(E_g+\hbar\omega)(3E_g+\hbar\omega)}+4\hbar^2\omega^2(\hbar^2\omega^2-E_g^2)}{8\hbar^2\omega^2(E_g+\hbar\omega)} \\ = & \frac{\sqrt{4\hbar^2\omega^2\left(E_g^2-\hbar^2\omega^2\right)^2+2e^2|\gamma_1|^2E_0^2(E_g+\hbar\omega)(3E_g+\hbar\omega)}+2\hbar\omega(\hbar^2\omega^2-E_g^2)}{4\hbar\omega(E_g+\hbar\omega)} \\ = & \sqrt{\frac{1}{4}\left(E_g-\hbar\omega\right)^2+\frac{e^2|\gamma_1|^2E_0^2(3E_g+\hbar\omega)}{8\hbar^2\omega^2(E_g+\hbar\omega)}}+\frac{1}{2}(\hbar\omega-E_g)\end{aligned} \tag{12}$$

When the photon energy is small ($\hbar\omega \ll E_g$), we can apply $\frac{E_g}{E_g^2-\hbar^2\omega^2} \simeq \frac{1}{E_g-\hbar\omega}$ and $\frac{1}{E_g-\hbar\omega} \simeq \frac{1}{E_g}(1+\frac{\hbar\omega}{E_g})$. So the behavior of ΔE can be estimated as

$$\begin{aligned}\Delta E &\simeq \sqrt{\frac{1}{4}\left(E_g-\hbar\omega\right)^2}+\frac{\frac{e^2|\gamma_1|^2E_0^2(3E_g+\hbar\omega)}{8\hbar^2\omega^2(E_g+\hbar\omega)}}{E_g-\hbar\omega}+\frac{1}{2}(\hbar\omega-E_g) \\ &= \frac{e^2|\gamma_1|^2E_0^2}{8\hbar^2\omega^2\left(E_g-\hbar\omega\right)}+\frac{e^2|\gamma_1|^2E_0^2E_g}{4\hbar^2\omega^2\left(E_g^2-\hbar^2\omega^2\right)} \\ &\simeq \frac{e^2|\gamma_1|^2E_0^2}{8\hbar^2\omega^2\left(E_g-\hbar\omega\right)}+\frac{e^2|\gamma_1|^2E_0^2}{4\hbar^2\omega^2\left(E_g-\hbar\omega\right)} \\ &\simeq \frac{3e^2|\gamma_1|^2E_0^2}{8\hbar\omega E_g}\left(\frac{1}{\hbar\omega}+\frac{1}{E_g}\right)\end{aligned} \tag{13}$$

As depicted by the dashed green line in Fig. S7, a decrease in photon energy $\hbar\omega$ results in a corresponding increase in the magnitude of the energy shift ΔE.

When the photon energy is approaching to band gap ($\hbar\omega \to E_g$), we estimate the behavior of ΔE as

$$\Delta E \simeq \frac{1}{4}\left(\frac{\hbar\omega(\hbar\omega-E_g)^2}{e|\gamma_1|E_0}+\frac{2e|\gamma_1|E_0}{\hbar\omega}+2(\hbar\omega-E_g)\right) \tag{14}$$

As shown by the dashed red line in Fig. S7, an increase in photon energy $\hbar\omega$ closed to the band gap E_g results in an increase in the magnitude of the energy shift ΔE.

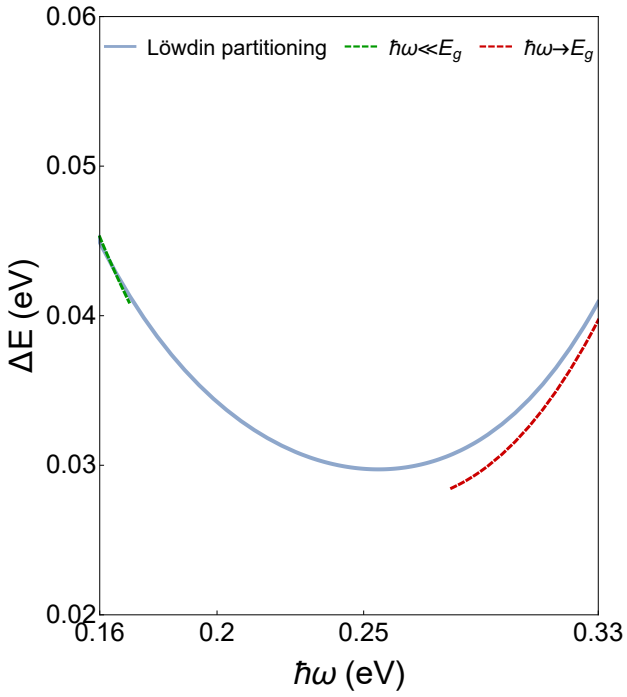

FIG. S7. **Comparison of perturbative results for the energy shift.** The blue curve for ΔE derived from the Löwdin partitioning approach, dashed green (red) line for the perturbative results for ΔE as the photon energy approaches 0.16 eV (the gap E_g).

Appendix I: Unresolved anti-crossing gap

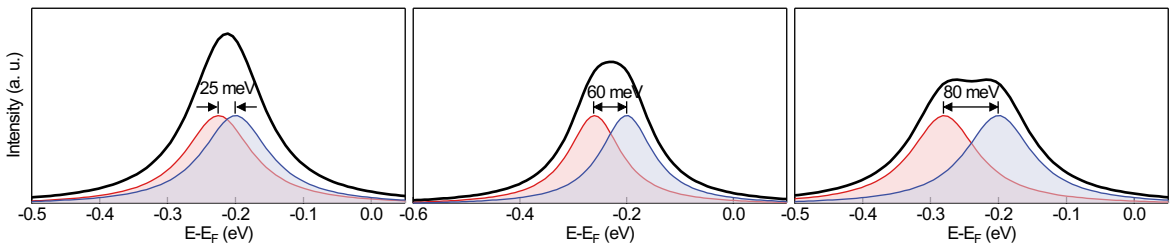

FIG. S8. Simulated EDC with different splitting sizes of 25, 60, and 80 meV. The FWHM of a single Lorentz peak (red and blue curves) is set to 100 meV similar to the experimental results. The splitting of 25 meV is too small to resolve.

We note that the anti-crossing gaps off the Γ point show up in the calculation in Fig. 4g,h,i,k of the main text, which are too small to be resolved in our TrARPES mea-

surement due to the band broadening (∼100 meV) from the sample and instrumentation limitation. As shown in the simulated EDC in Fig. S8, a separation of two peaks by 25 meV is too subtle to be resolved experimentally, when the peak width is 100 meV.

---

* These authors contributed equally to this work.

† peizhet@buaa.edu.cn

‡ syzhou@mail.tsinghua.edu.cn

[1] Georg Kresse and Jürgen Furthmüller. Efficient iterative schemes for ab initio total-energy calculations using a plane-wave basis set. *Phys. Rev. B*, 54(16):11169, 1996.

[2] Georg Kresse and Daniel Joubert. From ultrasoft pseudopotentials to the projector augmented-wave method. *Phys. Rev. B*, 59(3):1758, 1999.

[3] John P Perdew, Kieron Burke, and Matthias Ernzerhof. Generalized gradient approximation made simple. *Phys. Rev. Lett.*, 77(18):3865, 1996.

[4] Max Dion, Henrik Rydberg, Elsebeth Schröder, David C Langreth, and Bengt I Lundqvist. Van der Waals density functional for general geometries. *Phys. Rev. Lett.*, 92(24):246401, 2004.

[5] Jiří Klimeš, David R Bowler, and Angelos Michaelides. Van der Waals density functionals applied to solids. *Phys. Rev. B*, 83(19):195131, 2011.

[6] Aliaksandr V Krukau, Oleg A Vydrov, Artur F Izmaylov, and Gustavo E Scuseria. Influence of the exchange screening parameter on the performance of screened hybrid functionals. *J. Chem. Phys.*, 125(22):224106, 2006.

[7] Arash A Mostofi, Jonathan R Yates, Young-Su Lee, Ivo Souza, David Vanderbilt, and Nicola Marzari. wannier90: A tool for obtaining maximally-localised Wannier functions. *Comput. Phys. Commun.*, 178(9):685–699, 2008.

[8] Arash A Mostofi, Jonathan R Yates, Giovanni Pizzi, Young-Su Lee, Ivo Souza, David Vanderbilt, and Nicola Marzari. An updated version of wannier90: A tool for obtaining maximally-localised Wannier functions. *Comput. Phys. Commun.*, 185(8):2309–2310, 2014.

[9] Nicola Marzari, Arash A Mostofi, Jonathan R Yates, Ivo Souza, and David Vanderbilt. Maximally localized Wannier functions: Theory and applications. *Rev. Mod. Phys.*, 84(4):1419, 2012.

[10] Umberto De Giovannini, Shunsuke A Sato, Hannes Hübener, and Angel Rubio. First-principles modelling for time-resolved arpes under different pump–probe conditions. *J. Electron Spectrosc. Relat. Phenom.*, 254:147152, 2022.

[11] Umberto De Giovannini, Hannes Hübener, and Angel Rubio. Monitoring electron-photon dressing in WSe_2. *Nano Lett.*, 16(12):7993–7998, 2016.

[12] S. Ito, M. Schüler, M. Meierhofer, S. Schlauderer, J. Freudenstein, J. Reimann, D. Afanasiev, K. A. Kokh, O. E. Tereshchenko, J. Güdde, M. A. Sentef, U. Höfer, and R. Huber. Build-up and dephasing of Floquet–Bloch bands on subcycle timescales. *Nature*, 616:696, 2023.

[13] S. W. Jung, S. H. Ryu, W. J. Shin, Y. Sohn, M. Huh, R. J. Koch, C. Jozwiak, E. Rotenberg, A. Bostwick, and K. S. Kim. Black phosphorus as a bipolar pseudospin semiconductor. *Nat. Mater.*, 19(3):277–281, 2020.

[14] H. Yuan, X. Liu, F. Afshinmanesh, W. Li, G. Xu, J. Sun, B. Lian, A. G. Curto, G. Ye, Y. Hikita, Z. Shen, S. C. Zhang, X. Chen, M. Brongersma, H. Y. Hwang, and Y. Cui. Polarization-sensitive broadband photodetector using a black phosphorus vertical p-n junction. *Nat. Nanotechnol.*, 10(8):707–13, 2015.

[15] Fahad Mahmood, Ching-Kit Chan, Zhanybek Alpichshev, Dillon Gardner, Young Lee, Patrick A Lee, and Nuh Gedik. Selective scattering between Floquet-Bloch and Volkov states in a topological insulator. *Nat. Phys.*, 12(4):306, 2016.

[16] Guowei Zhang, Shenyang Huang, Andrey Chaves, Chaoyu Song, V Ongun Özçelik, Tony Low, and Hugen Yan. Infrared fingerprints of few-layer black phosphorus. *Nat. Commun.*, 8(1):14071, 2017.

[17] Motohiko Ezawa. Topological origin of quasi-flat edge band in phosphorene. *New J. Phys.*, 16(11):115004, 2014.

[18] Narges Kafaei and Mohammad Sabaeian. Two-band kp hamiltonian of phosphorene based on the infinitesimal basis transformations approach. *Superlattices Microstruct.*, 109:330–336, 2017.

[19] Roland Winkler. *Spin-orbit coupling effects in two-dimensional electron and hole systems*, volume 191. Springer, 2003.